RSC Advances

PAPER

View Article Online
View Journal | View Issue

Cite this: *RSC Adv.*, 2020, **10**, 23372

Synthesis, crystal structures, and luminescent properties of Zn(II), Cd(II), Eu(III) complexes and detection of Fe(III) ions based on a diacylhydrazone Schiff base†

Aiying Han, Hao Su, Guohong Xu, Maroof Ahmad Khan and Hui Li *

Received 23rd April 2020
Accepted 13th June 2020

DOI: 10.1039/d0ra03642k

rsc.li/rsc-advances

Acylhydrazone Schiff bases are rich in N and O atoms to coordinate with metal ions to form multidentate complexes. In this study, a novel diacylhydrazone Schiff base (N'^1E,N'^4E)-N'^1,N'^4-bis(2-hydroxy-5-nitrobenzylidene)succinohydrazide (H_4L) was synthesized from the condensation of nitrosalicylaldehyde and succinic dihydrazide. The interactions of H_4L with common monovalent, divalent and trivalent metal ions were investigated by ultraviolet spectroscopy and fluorescence spectroscopy. The results showed that H_4L had no obvious effect on the monovalent metal ions (Li^+, Na^+, K^+), but reacted with most divalent and trivalent metal ions, and showed single selectivity in the fluorescence recognition of Fe^{3+} ions. More importantly, three kinds of binuclear molecular structures, $[Zn_2(H_2L)_2]\cdot 5DMF$ (**Zn-L**), $[Cd_2(H_2L)_2]\cdot DMF\cdot H_2O$ (**Cd-L**) and $[Eu_2(H_2L)_3]\cdot 6DMSO$ (**Eu-L**), have been studied to further illustrate the interaction mode of diacylhydrazone Schiff base and metal ions. In addition, the optical properties of these crystallized complexes have been studied in DMF solution.

Introduction

The acylhydrazone Schiff base is the product formed by condensation reaction of hydrazine derivatives with aldehydes or ketone derivatives.[1] According to the number of acylhydrazone groups (–NH–CO–), it can be divided into monoacylhydrazone, diacylhydrazone and polyacylhydrazone Schiff base. As a peculiar kind of Schiff base, the diacylhydrazone Schiff base formed by succinic dihydrazide not only shows good stability because of the p–π conjugated system[2,3] but also provides greater flexibility in three-dimensional space on account of the free rotation of the C–C single bond in the succinoyl fraction[4] so that this kind of ligand exhibits strong coordination abilities and good characteristics of forming a variety of complex structures. Particularly, acylhydrazone metal complexes have found extensive application in diverse fields, such as magnetism,[5–8] catalytic performance,[9–12] biological function[13,14] and molecular recognition.[15–18] And the application of rare earth metal complexes in ion recognition has attracted more and more attention due to their near infrared luminescence properties.[19,20] Scores of acylhydrazone metal complexes based on aromatic rings have been reported in the past few years. Nevertheless, merely a few studies on metal complexes of diacylhydrazone Schiff base containing flexible C–C single bond in the molecule, especially rare earth metal complexes have been reported. In 2013, Duan's group reported three kinds of diacylhydrazone Schiff bases and got their complexes based on Ce(III), which can be used to recognize Mg^{2+} and Al^{3+}, respectively.[21]

In recent years, we have designed and synthesized series of monoacylhydrazone Schiff bases in our group. A variety of transition metals complexes based on them have indicated that this kind of ligands possessed the advantage of constructing different forms of structures.[22–25] To extend our research, we designed and synthesized a new diacylhydrazone Schiff base (N'^1E,N'^4E)-N'^1,N'^4-bis(2-hydroxy-5-nitrobenzylidene)succinohydrazide (**H_4L**) (Scheme 1) by the condensation of nitrosalicylaldehyde and succinic dihydrazide. Even more importantly, we got three novel binuclear complexes **Zn-L**, **Cd-L**, **Eu-L**, and studied the structures and optical properties of them. It was worth mentioning that Zn(II) and Cd(II) are coordinated with two

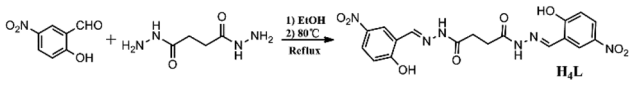

Scheme 1 Synthetic route of H_4L.

Key Laboratory of Cluster Science of Ministry of Education, School of Chemistry and Chemical Engineering, Beijing Institute of Technology, Beijing 100081, P. R. China. E-mail: lihui@bit.edu.cn

† Electronic supplementary information (ESI) available: Details about general methods, structure information, spectra (^1H, ^{13}C NMR, IR, UV-vis, fluorescence, mass spectra), PXRD, thermogravimetric analysis. CCDC 1989009–1989011. For ESI and crystallographic data in CIF or other electronic format see DOI: 10.1039/d0ra03642k

ligands to form butterfly-like structures while Eu(III) is coordinated with three ligands to form a complex with a cavity in the middle.

Herein, we also investigated the interaction of **H_4L** with common metal ions by using ultraviolet spectroscopy and fluorescence spectrum, and found that **H_4L** has a distinct fluorescence quenching in the presence of Fe^{3+} ions. Already well known, Fe^{3+} ions play critical roles in living organisms, and are essential elements in many biochemical process.[26–29] However, excess iron ions in human body will cause hemochromatosis and diabetes *etc.*[30] Moreover, for **H_4L**, its molecular structure is relatively simple, and the synthesis only requires one step of reaction. These advantages confirm its potential in the practical application of Fe^{3+} detection in the future.

Experimental

Materials and measurements

All chemicals used in synthesis were obtained from commercial sources without further refinement. FT-IR spectrum was recorded in the VERTEX 80V FT-IR spectrometer as KBr pellets in the 4000–400 cm^{-1} region. ^{1}H NMR and ^{13}C NMR spectra were recorded on a Bruker ARX400 spectrometer (400 MHz) instrument in DMSO-d^6 with Me_4Si as the internal standard. The UV-vis absorption spectra were examined on a PERSEE TU-1950 spectrophotometer in the wavelength range of 190–650 nm and the solvent used to register the UV-visible spectra was DMF solution. The photoluminescence spectra were recorded by using a Hitachi F-7000 luminescence spectrophotometer equipped with a 450 W xenon lamp as the excitation source. The photomultiplier tube voltage was 700 V, the scan speed was 1200 nm min^{-1}, and the slit width was 5.0 nm. The powder X-ray diffraction (PXRD) patterns of the samples were measured using a Japan Rigaku D/Max γ A X-ray diffractometer equipped with graphitemonochromatized Mo-Kα radiation (λ = 0.71073 Å). Thermo-gravimetric analyses (TGA) were carried out on a SEIKO TG/DTA 6200 thermal analyzer from room temperature to 650 °C at a ramp rate of 10 °C min^{-1} in a flowing 50 mL min^{-1} nitrogen atmosphere. The mass spectra was recorded by using an AGILENT Liquid Chromatograph Mass Spectrometer (Q-TOF 6520).

Preparation of the ligand H_4L

An ethanol (20 mL) solution of 5-nitrosalicylaldehyde (3.677 g, 20 mmol) was added dropwise to an ethanol (20 mL) solution of succinic dihydrazide (1.462 g, 10 mmol) with stirring ceaselessly. The addition of one drop of concentrated hydrochloric acid induced a color change to yellow along with immediate precipitation. After that, the mixture was refluxed for 8 hours with continuous stirring and subsequently cooled to room temperature. A yellow solid was collected by vacuum filtration, washed with ethanol and diethyl ether several times, and dried in air. Yield: (73%). Element analysis results of $C_{18}H_{16}N_6O_8$ (444.10), theoretical value (%): C, 48.65; H, 3.63; N, 18.91. Experimental value (%): C, 48.83; H, 3.72; N, 18.44. Selected IR (KBr pellet, cm^{-1}): ν (O–H) 3288; ν (C=O) 1647; ν (C=N) 1557(s). ^{1}H NMR (400 MHz, DMSO-d^6) δ (ppm) 12.31 (s, 2H), 11.92 (s, 2H), 9.09 (s, 2H), 8.54–8.46 (m, 4H), 7.18–7.05 (m, 2H), 3.00 (t, J = 4.0 Hz, 2H), 2.60 (t, J = 4.0 Hz, 2H). ^{13}C NMR (175 MHz, DMSO-d^6) δ (ppm) 175.61, 174.16, 168.79, 168.45, 164.16, 162.97, 162.19, 160.51, 143.13, 140.32, 137.98, 137.80, 128.65, 126.74, 124.39, 117.83, 29.17, 27.18.

Preparation of complexes

A solution of **H_4L** (22 mg, 0.05 mmol) in 2 mL DMF containing 20 drops of NaOH (0.1 M) methanol was added in the solution of $Zn(NO_3)_2\cdot 6H_2O$ (30 mg, 0.1 mmol) in 9 mL of methanol with continuous stirring for *ca.* 30 min. Then, the resulting solution was filtered and remained undisturbed at room temperature to give a yellow solution. A yellow single crystal suitable for X-ray analysis was produced by slow evaporation of mother liquor for three days. For $C_{51}H_{63}Zn_2N_{17}O_{21}$ (**Zn-L**), yield: 69%.

A solution of **H_4L** (22 mg, 0.05 mmol) in 3 mL DMF containing 30 drops of NaOH (0.1 M) methanol was added in the solution of $Cd(NO_3)_2\cdot 4H_2O$ (31 mg, 0.1 mmol) in 8 mL of methanol with continuous stirring for ca. 30 min. The resulting solution was then filtered and remained undisturbed at room temperature. A yellow green single crystal suitable for X-ray analysis was produced by slow evaporation of mother liquor for three days. For $C_{39}H_{37}Cd_2N_{13}O_{18}$ (**Cd-L**), yield: 67%.

A solution of $Eu(CH_3COO)_3\cdot H_2O$ (12 mg, 0.05 mmol) in 3 mL DMSO was added by solution of **H_4L** (13 mg, 0.05 mmol) in 3 mL DMSO. The reaction solution was filtrated after stirring with ca. 20 min. Yellow single crystals suitable for X-ray diffraction analysis were obtained from isopropanol vapor diffusion into the filtrate for several days. For $C_{66}H_{78}Eu_2N_{18}O_{30}S_6$ (**Eu-L**), yield: 78%.

Table 1 Crystal data and structure refinement of the complexes

Complexes	Zn-L	Cd-L	Eu-L
Formula	$C_{51}H_{63}Zn_2N_{17}O_{21}$	$C_{39}H_{37}Cd_2N_{13}O_{21}$	$C_{66}H_{69}Eu_2N_{18}O_{30}S_6$
M/mol^{-1}	1380.92	1248.61	2090.67
T/K	153(2)	153(2)	296(2)
Crystal system	Monoclinic	Triclinic	Orthorhombic
Space group	$C2/c$	$P\bar{1}$	$Pbcn$
a/Å	15.6845(13)	12.091(2)	27.308(6)
b/Å	18.3664(15)	12.459(3)	19.968(5)
c/Å	21.3297(12)	17.130(3)	16.327(3)
α/°	90	90.42(3)	90
β/°	100.584(7)	104.13(3)	90
γ/°	90	95.41(3)	90
V/Å^3	6039.8(8)	2490.0(9)	8903(3)
Z	8	2	4
ρ/mg·cm^{-3}	1.519	1.665	1.560
μ(Mo-Kα)/mm^{-1}	0.885	0.945	1.623
F (000)	2864	1252	4212
S (GOF)	1.043	1.042	1.031
$R_1[I > 2\sigma(I)]$	0.0570	0.0377	0.0728
w$R_2[I > 2\sigma(I)]$	0.1026	0.1003	0.1676
$\Delta\rho_{max,\ min}$/eÅ^{-3}	0.979, −1.010	1.444, −0.552	1.640,−1.141

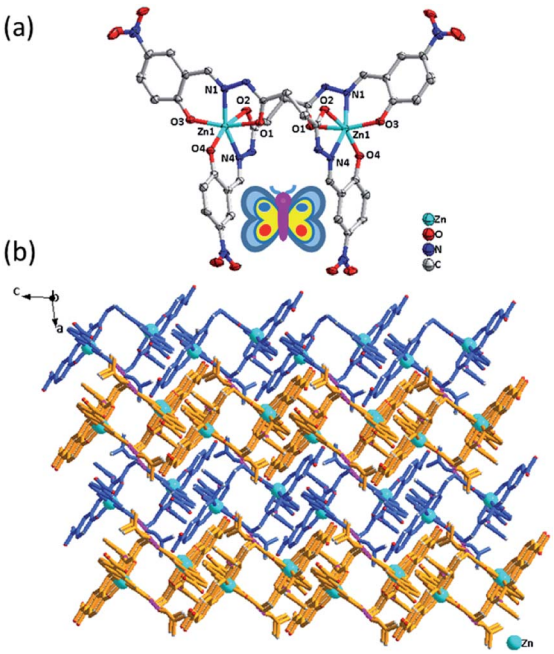

Fig. 1 Crystal structure of **Zn-L**. (a) ORTEP picture of binuclear **Zn-L** combined with coordination bond, solvent molecules and anions are omitted for clarity, (b) the H-bonding linking the molecule of DMF with the binuclear structure (purple dashed lines) and 3D supramolecular structure of **Zn-L** from *b* axis.

X-ray crystal structure determinations

Diffraction intensity for the complexes were collected on a Rigaku RAXIS-RAPID CCD diffractometer equipped with a graphitemonochromatic MoKα radiation (l $\frac{1}{4}$ 0.71073 Å) using a ω scan mode at 153 ± 2 K (complexes **Zn-L** and **Cd-L**), 296 ± 2 K (**Eu-L**). The structures were solved by direct methods and refined using full-matrix least square techniques on F^2 with the program SHELXL (complexes **Cd-L** and **Eu-L**) and Olex2 (three complexes). Crystallographic data were shown in Table 1.

Results and discussion

Crystal structure of $[Zn_2(H_2L)_2]\cdot 5DMF$ (Zn-L)

X-ray crystallographic analysis reveals that **Zn-L** crystallizes in the monoclinic space group *C*2/*c*. As shown in Fig. 1, the binary core unit of **Zn-L** contains two Zn(II) ions, two partially deprotonated $[H_2L]^{2-}$ ligands and five solvent DMF molecules. Moreover, it possesses a 2-fold axis of symmetry, in addition the atoms N9, C29 of one DMF molecule lies on the 2-fold axis. Each Zn(II) shows 6-coordination with O on the two phenolic hydroxyl groups, N on the imines and O on the two carbonyl groups of two ligands to form stable five-membered rings and six-membered rings. The coordination environment is $Zn–N_2O_4$, including Zn–O bonds fall in the range 2.016(Zn1–O3) to 2.243(Zn1–O2) Å and Zn–N fall in the range 2.086 (Zn1–N1) to 2.088 (Zn1–N4) Å to form a rhombic metallacycle with a Zn⋯Zn separation of 6.44 Å, making the double-nucleus structure looks like a butterfly. The dihedral angles between the two tridentate chelators in one bridge ligand both are about 88°. There are almost only Van der Waals interactions between the binuclear complexes to arrange into 3D structure. The free DMF molecules exist in the structure by forming hydrogen bonds with uncoordinated N on the amide groups in the ligands.

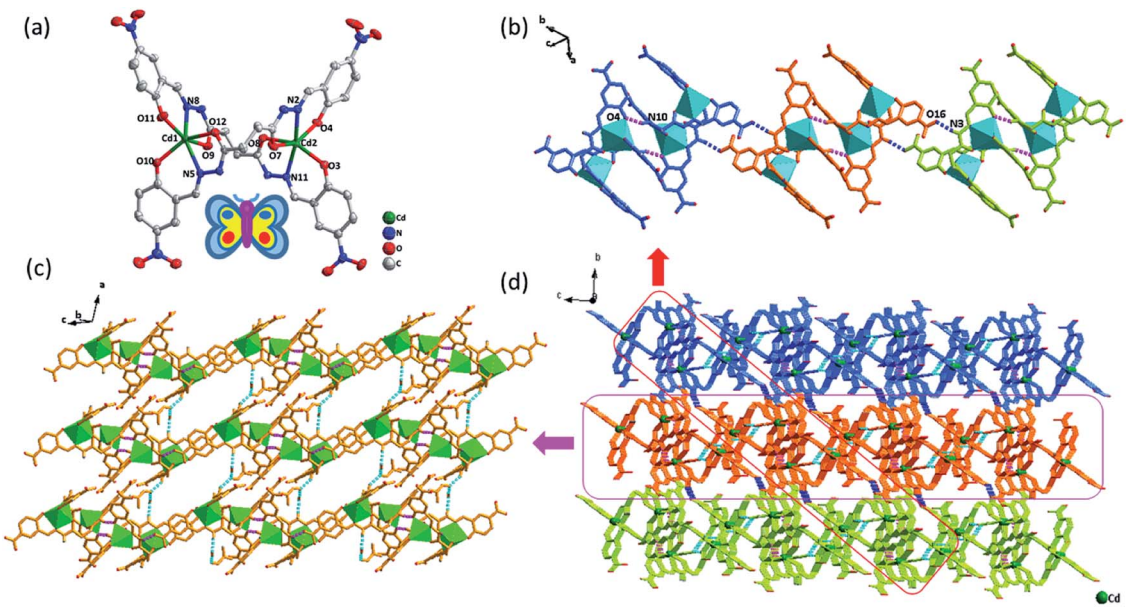

Fig. 2 Crystal structure of **Cd-L**. (a) ORTEP picture of binuclear **Cd-L** combined with coordination bond, solvent molecules and anions are omitted for clarity, (b) The H-bonding linking between binuclear structures to form dimer (N10–H10⋯O4: purple dashed lines)and 1D chain structure (N3–H3⋯O16: blue dashed lines) of **Cd-L**, (c) 2D plane linked by four kinds of hydrogen bonding (light blue dashed lines), (d) 3D supramolecular structure of **Cd-L** from *a* axis.

Crystal structure of $[Cd_2(H_2L)_2]\cdot DMF\cdot H_2O$ (Cd-L)

As shown in Fig. 2, X-ray crystallographic analysis reveals that **Cd-L** is a binuclear molecule and crystallizes in the triclinic space group $P\bar{1}$, and the binary core unit contains two Cd(II) ion, two partially deprotonated $[H_2L]^{2-}$ ligands, solvent DMF molecules (including a partially occupied and unordered DMF) and H_2O molecule. Similar to complex **Zn-L**, each Cd(II) exhibits 6-coordination with O on two phenolic hydroxyl groups, N on two imines and O on two carbonyl groups in two ligands to form stable five-membered rings and six-membered rings in the coordination environment of Cd–N_2O_4. The dihedral angles between the two tridentate chelators in one bridge ligand are about 85° and 80°, respectively. Thus, **Cd-L** demonstrates the similar double-nucleus structure with butterfly shape and the distance of Cd···Cd is *ca.* 6.54 Å. The four uncoordinated imine groups don't deprotonate, making them easy to be donors of hydrogen bonds. N10 on imine group of the binuclear structure and O4 on phenolic hydroxyl in the other binuclear unit form an N–H···O hydrogen bond to come into being dimers. The distance between adjacent Cd in the two binuclear structures forming dimer is about 6.01 Å. Furthermore, each dimer interacts with two neighbours to form 1D chains by H-bonding between imine and terminal nitro group (N3–H3···O16: 2.049, 2.808, 141.31). In addition, the adjacent 1D chains are further assembled by four kinds of hydrogen bonds (N4–H4···O17: 2.056, 2.835, 144.15; N9–H9···O18: 2.013, 2.791, 144.15; O18–H18A···O17: 1.975, 2.824, 177.94; O18–H18···O10: 1.963, 2.813, 177.32) between ligands, DMF and H_2O (Fig. 2c) to form a 3D supramolecular structure (Fig. 2d).

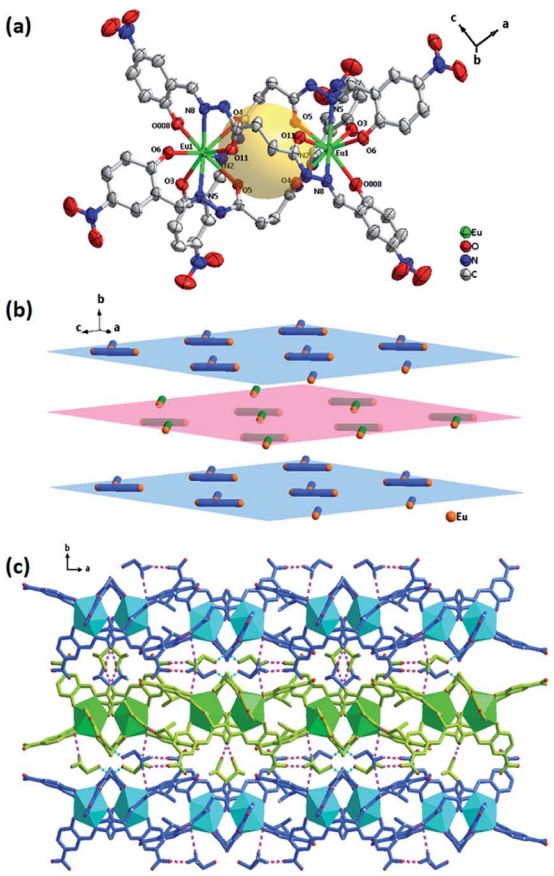

Fig. 3 Crystal structure of **Eu-L**. (a) ORTEP picture of binuclear **Eu-L** combined with coordination bond, solvent molecules and anions are omitted for clarity, (b) simplified stacking diagram of **Eu-L**, the metal is drawn in orange, the virtual bond between Eu(III) of one binuclear is drawn in blue and green respectively, (c) 3D supramolecular structure linked by hydrogen bonding (C–H···O: purple dashed lines; N–H···O: light blue dashed lines)of **Eu-L** from *c* axis. The different colors represent different layers.

Crystal structure of $[Eu_2(H_2L)_3]\cdot 6DMSO$ (Eu-L)

A single crystal X-ray analysis of compound **Eu-L** reveals that it crystallizes in the orthorhombic space group *Pbcn*. As shown in Fig. 3, the molecule of the compound **Eu-L** comprises three deprotonated ligands and two Eu(III) ions. The two Eu(III) ions are coordinated with three equivalent NOO tridentate chelators of three ligands to form a three-crown structure at both ends that cannot completely overlap, which shows that **Eu-L** doesn't have an ideal C_3 symmetry (Fig. S3†). In fact, the compound **Eu-L** just possesses a 2-fold axis of symmetry. Each ligand bridges two Eu(III) ions in a twist manner with the Eu···Eu separation being 6.5219(12) Å. Three dihedral angles between the two tridentate chelators in one bridge ligand is about 86°, 83° and 80°. The opening of the cavity within the binuclear structure is a rhombus of size about 6.8 × 6.5 $Å^2$. The radius of the cavity is about 2.25 Å, and the closed separation from the cavity center to the oxygen atom of the carbonyl in the ligand is about 2.30 Å.

Interestingly, the binuclear structures are interlaced with each other (Fig. 3b) and interconnected by nonclassical hydrogen bonds such as C–H···O interaction (C30–H30C···O6 2.629 3.528 156.13; C29–H29B···O2 2.302 3.203 155.95) between the -OH_{phenol} and the methyl of DMSO to form 2D sheets. Then each layer is further connected by the N–H···O interaction involving the amide N–H and the O of the DMSO extending the network in the three dimension. This 3D framework architecture is further supported by the hydrogen bonds of binuclear structures with other two DMSO molecules (Fig. 3c).

As a complement, the lengths (Å) and angles (deg) of hydrogen bonds and selected bonds data for the complexes **Zn-L**, **Cd-L** and **Eu-L** can be seen in Tables S1–S4†. The structures from the other viewing direction of **Zn-L**, **Cd-L** and **Eu-L** are shown in Fig. S4–S6.†

Powder X-ray diffraction (PXRD) analysis

To prove the purity and crystallinity of the bulk materials, the three complexes were employed towards the PXRD analysis, shown in Fig. 4. Notably, the experimental PXRD pattern of **Zn-L**, **Cd-L** and **Eu-L** matches quite well with that of the simulated pattern obtained from the Mercury, which shows rational crystalline phase purity of the bulk sample.

Optical properties

UV-vis absorption studies of ligand and complexes. The ligand H_4L and complexes have good solubility in DMF solution. The UV-vis spectrum of the free H_4L in DMF solution

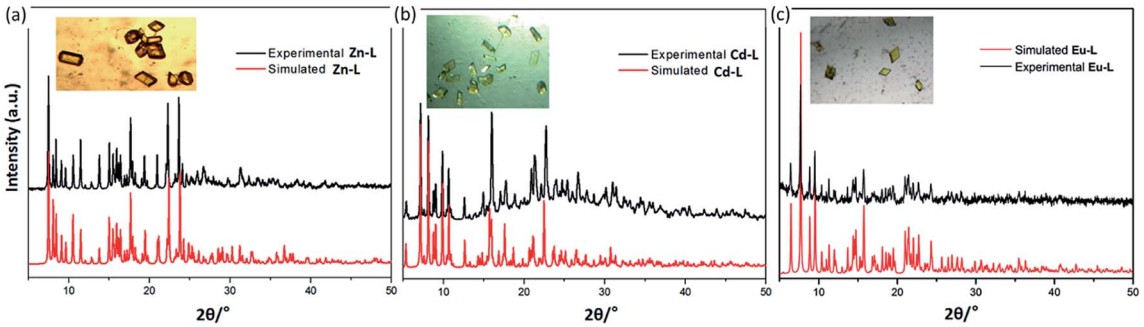

Fig. 4 The XRPD patterns of complexes **Zn-L**, **Cd-L** and **Eu-L**.

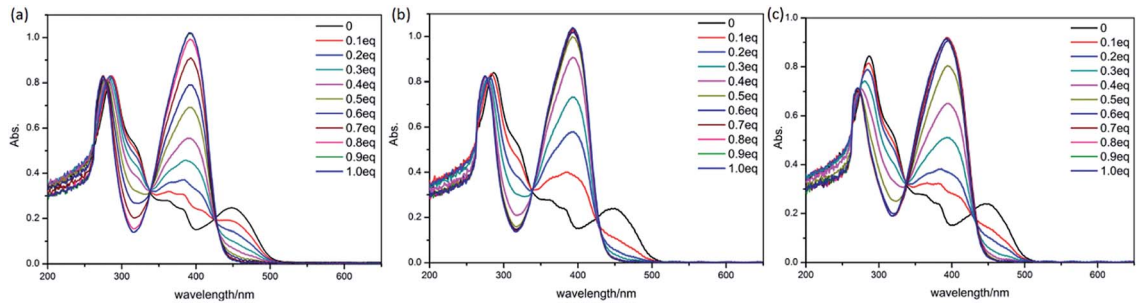

Fig. 5 UV-vis titration spectra of Zn^{2+} (a), Cd^{2+} (b) and Eu^{3+} (c) to H_4L in DMF.

exhibits a major absorption band at 287 nm attributed to the conjugate system formed by the co-plane of benzene ring and C=N bond, the maximum absorption peak (λ_{max}) located at 450 nm corresponding to the π–π* and n–π* transitions.[31] The addition of divalent metal ions(Ca^{2+}, Mg^{2+}, Ba^{2+}, Mn^{2+}, Co^{2+}, Cu^{2+} and Zn^{2+}) and trivalent metal ions(Al^{3+}, Cr^{3+}, Fe^{3+} and Eu^{3+}) to the solution of **H_4L** (20 μM) significantly change the λ_{max} of pure **H_4L** (Fig. S8†). Remarkably, it shows same equivalence points after the addition of Eu^{3+} compared with divalent metal ions, such as Zn^{2+}, indicating the similar coordination pattern between them (see Fig. 5). It can clearly be seen that the result matches the UV-vis spectrum of the complexes, and is consistent with the previous structural analysis. Whereas the addition of monovalent cations (Li^+, Na^+ and K^+) to the **H_4L** solution do not impose obvious change to the absorption spectrum.

Fluorescent properties of ligand and complexes. The photoluminescent behaviours of three complexes as well as the free ligand **H_4L** were investigated in the solution of DMF at room temperature (Fig. 6). The fluorescence emission spectra of pure **H_4L** exhibits dual emission at λ_{em} values of 320 nm (accompanied by two shoulder peaks at 307 nm, 331 nm) and 417 nm, upon irradiation at 290 nm, which may be caused by the π–π* transition of the conjugated system in the Schiff base ligand. Apparently, the emission of complexes **Zn-L** and **Cd-L** are similar to that of the ligand, and the emission at 424 nm of complex **Eu-L** is similar to that of the ligand, indicating that the binuclear complexes have an L-based emission. As for the complex **Zn-L**, compared to the free ligand, the intensity of the

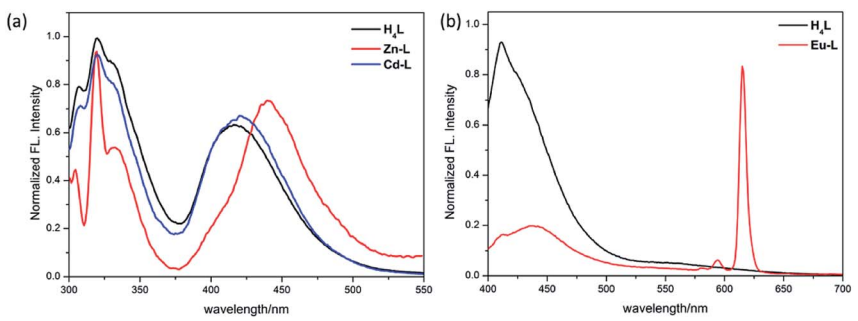

Fig. 6 PL spectra of **H_4L**, **Zn-L**, **Cd-L** in DMF with 20 mM (λ_{ex} = 290 nm) (a), PL spectra and photos of **H_4L** and **Eu-L** in DMF with 20 Mm (λ_{ex} = 390 nm) (b).

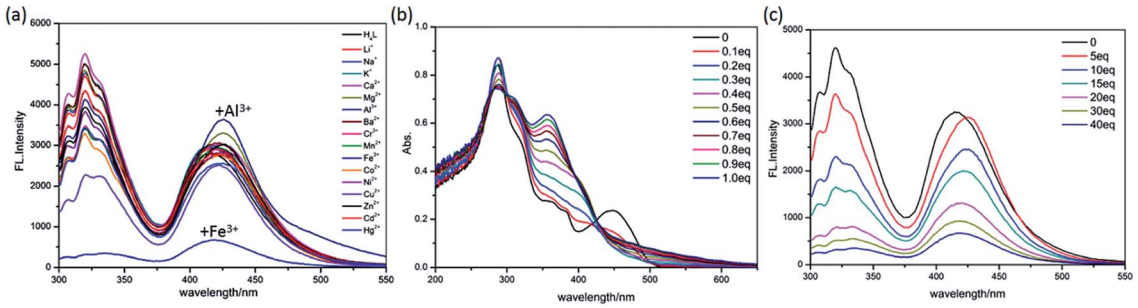

Fig. 7 Fluorescence intensity after adding 40 equiv. of different metal ions to H_4L solution (2×10^{-5} M, DMF) ($\lambda_{ex} = 290$ nm) (a); UV-vis titration spectra of Fe^{3+} to H_4L in DMF (b); The change of the fluorescence spectra of H_4L (2×10^{-5} M, DMF) upon gradual addition of Fe^{3+} ions (c).

shoulder peaks is reduced, and the peak at 420 nm has a visible redshift, which can be attributed to π–π* intraligand (IL) transitions of the ligand and ligand-to-metal charge transfer.[22] Fluorescence spectra of **Cd-L** shows similar changes with **Zn-L**, which may be due to their similar molecular structures.[32] Due to the complexation of H_4L with Eu(III) ions, the intensity of the peak at 417 nm is reduced, accompanied by a slight redshift, and a new peak centred on $\lambda_{em} = 615$ nm appears, which is the characteristic peak of the Eu(III) complex.[33,34] In the meanwhile, the complex **Eu-L** exhibits a red luminescence while the free ligand H_4L shows a blue-green luminescence in DMF solution under the irradiation of $\lambda = 375$ nm ultraviolet light.

Fluorescence recognition of Fe^{3+} ions

As shown in Fig. 7a, after the addition of different metal ions including Li^+, Na^+, K^+, Ca^{2+}, Mg^{2+}, Ba^{2+}, Al^{3+}, Cr^{3+}, Mn^{2+}, Fe^{3+}, Co^{2+}, Ni^{2+}, Cu^{2+}, Zn^{2+}, Cd^{2+} and Hg^{2+} to H_4L solutions, only Fe^{3+} ions cause the apparent fluorescence quenching of H_4L. Differently, the addition of Mg^{2+}, Al^{3+}, Zn^{2+} result in different degrees of weak fluorescence enhancement.

Although the single crystal structure of Fe-L has not been obtained after many efforts on preparing high quality of single crystals, the coordination interaction between Fe^{3+} and H_4L has been investigated by UV-vis titration of H_4L (20 μM) by incremental addition of Fe^{3+} ions (0.03 M) in DMF solution (Fig. 7b). By addition of Fe^{3+} ions into H_4L, the absorption band of H_4L at 450 nm disappears. These changes are along with the appearance of two clear isosbestic points at 425 nm and 495 nm. Moreover, the absorption band of H_4L at 287 nm shows a slight redshift. These changes are accompanied by the appearance of two clear isosbestic points at 270 nm and 290 nm, which indicate that Fe^{3+} ions complexed with H_4L.

The turn-off of the fluorescence of H_4L by Fe^{3+} ions is explained with the help of a fluorescence emission titration (Fig. 7c). Addition of incremental amounts of Fe^{3+} ions lead to a fluorescence quenching of the ligand solution, which may be caused by the complexation of H_4L with Fe^{3+} ions, resulting in the charge transfer from ligand to the half-filled 3d orbital of Fe^{3+} ions.[35,36] As shown in the mass spectra (Fig. S9†), the peak assigned to $[Fe_2(HL)_2\text{-}H^+]^+$ helps us to speculate the coordination mode of H_4L with Fe^{3+} ions in solution, which is similar

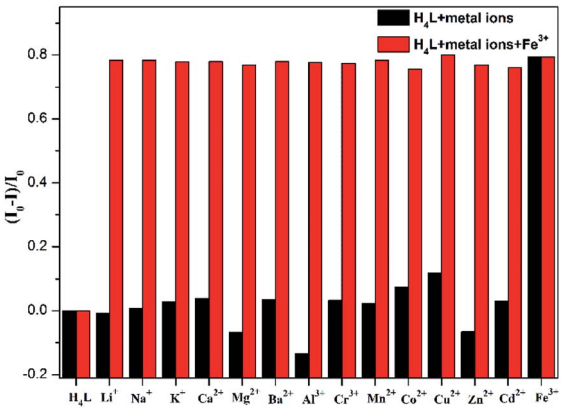

Fig. 8 Fluorescence intensity at 420 nm of H_4L (in DMF solution, 20 μM) containing 40 equiv. of iron ions and 40 equiv. of other competing ions. *I*0 represents the fluorescence intensity of the ligand solution, and *I* represents the fluorescence intensity of the solution after adding metal ions.

with complexes **Zn-L**, **Cd-L** and **Eu-L** with single crystal structural analysis comprehensively (Fig. S10†). In addition, anti-interference experiment (Fig. 8) reveals the absence of any interference with the detection of Fe^{3+} ions by the inclusion of metal ions, indicating the excellent selectivity of H_4L for Fe^{3+} ions.

Conclusions

In summary, we have successfully demonstrated the synthesis and characterizations of a new diacylhydrazone Schiff base (H_4L), which contains Schiff base (–CH═N–), imine group (–NH), nitro group ($-NO_2$) and phenolic hydroxyl group (–OH). It can nicely coordinate with divalent and trivalent metal ions. In addition, three new binuclear coordination compounds namely **Zn-L**, **Cd-L** and **Eu-L** have been synthesized based on H_4L. Among them, Zn(II) or Cd(II) can coordinate with two ligands respectively to show a butterfly shape, while Eu(III) can coordinate with three ligands. What's more, the ligand H_4L shows a "turn-off" fluorescence sense for Fe^{3+} ions in DMF solution with high selectivity, which provides a potential of detection applications in the future.

Conflicts of interest

The authors confirm that there are no conflicts of interest to declare.

Acknowledgements

This work was financially supported by the National Natural Science Foundation of China (No. 21471017).

References

1 J. Fan, S. Zhang, Y. Xu, N. Wei, B. Wan, L. Qian and Y. Liu, *Carbohydr. Polym.*, 2020, **228**, 115379.
2 R. Dwivedi, D. P. Singh, S. Singh, A. K. Singh, B. S. Chauhan, S. Srikrishna and V. P. Singh, *Org. Biomol. Chem.*, 2019, **17**, 7497–7506.
3 L. Wu, P. Wu, D. Guo, W. Fu, D. Li and T. Luo, *Croat. Chem. Acta*, 2015, **88**, 1–6.
4 R. Borthakur, A. Kumar and R. A. Lal, *Spectrochim. Acta, Part A*, 2014, **118**, 94–101.
5 A. Adhikary, S. Goswami, J. A. Sheikh and S. Konar, *Eur. J. Inorg. Chem.*, 2014, **2014**, 963–967.
6 S. Xue, L. Zhao, Y. N. Guo and J. Tang, *Dalton Trans.*, 2012, **41**, 351–353.
7 A. Adhikary, J. A. Sheikh, S. Biswas and S. Konar, *Dalton Trans.*, 2014, **43**, 9334–9343.
8 U. Golla, A. Adhikary, A. K. Mondal, R. S. Tomar and S. Konar, *Dalton Trans.*, 2016, **45**, 11849–11863.
9 S. D. Kurbah, A. Kumar, I. Syiemlieh, M. Asthana and R. A. Lal, *Inorg. Chem. Commun.*, 2017, **86**, 39–43.
10 R. Arunachalam, E. Chinnaraja, A. Valkonen, K. Rissanen, S. K. Sen, R. Natarajan and P. S. Subramanian, *Inorg. Chem.*, 2018, **57**, 11414–11421.
11 C. He, J. Wang, L. Zhao, T. Liu, J. Zhang and C. Duan, *Chem. Commun.*, 2013, **49**, 627–629.
12 W. Zhu, X. Wu, C. He and C. Duan, *Tetrahedron*, 2013, **69**, 10477–10481.
13 S. D. Kurbah, A. Kumar, I. Syiemlieh and R. A. Lal, *Polyhedron*, 2018, **139**, 80–88.
14 Q. Yao, J. Qi, Y. Zheng, K. Qian, L. Wei, M. Maimaitiyiming, Z. Cheng and Y. Wang, *J. Inorg. Biochem.*, 2019, **193**, 1–8.
15 S. Chopra, J. Singh, H. Kaur, A. Singh, N. Singh and N. Kaur, *Eur. J. Inorg. Chem.*, 2015, **2015**, 4437–4442.
16 K. Santhiya, S. K. Sen, R. Natarajan, R. Shankar and B. Murugesapandian, *J. Org. Chem.*, 2018, **83**, 10770–10775.
17 S. Gao, L. Li, I. Vohra, D. Zha and L. You, *R. Soc. Open Sci.*, 2017, **4**, 170466.
18 X. Ma, Y. Cui, S. Liu and J. Wu, *Soft Matter*, 2017, **13**, 8027–8030.
19 D. Shi, X. Yang, H. Chen, Y. Ma, D. Schipper and R. A. Jones, *J. Mater. Chem. C*, 2019, **7**, 13425–13431.
20 D. Shi, X. Yang, Z. Xiao, X. Liu, H. Chen, Y. Ma, D. Schipper and R. A. Jones, *Nanoscale*, 2020, **12**, 1384–1388.
21 L. Zhao, Y. Liu, C. He, J. Wang and C. Duan, *Dalton Trans.*, 2014, **43**, 335–343.
22 B.-b. Tang, H. Ma, G.-z. Li, Y.-b. Wang, G. Anwar, R. F. Shi and H. Li, *CrystEngComm*, 2013, **15**, 8069–8073.
23 B.-b. Tang, X.-p. Sun, G.-l. Liu and H. Li, *J. Mol. Struct.*, 2010, **984**, 111–116.
24 G. Xu, B. Tang, L. Gu, P. Zhou and H. Li, *J. Mol. Struct.*, 2016, **1120**, 205–214.
25 G. Xu, B.-b. Tang, L. Hao, G.-l. Liu and H. Li, *CrystEngComm*, 2017, **19**, 781–787.
26 J. Kaplan and D. M. Ward, *EBioMedicine*, 2015, **2**, 1582–1583.
27 P. T. Lieu, M. Heiskala, P. A. Peterson and Y. Yong, *Mol. Aspect. Med.*, 2001, **22**, 1–87.
28 M. A. Alam, T. K. Pal, M. A. Mumit and M. A.-A.-A.-A. Islam, *J. Sci. Res.*, 2012, **4**, 635–647.
29 X. Gong, X. Ding, N. Jiang, T. Zhong and G. Wang, *Microchem. J.*, 2020, **152**, 104351.
30 M. W. Hentze, M. U. Muckenthaler, B. Galy and C. Camaschella, *Cell*, 2010, **142**, 24–38.
31 D. Zhang, W. Zhao, Z. Feng, Y. Wu, C. Huo, L. He and W. Lu, *E-Polymers*, 2019, **19**, 15–22.
32 D. Majumdar, D. Das, S. S. Sreejith, S. Nag, S. Dey, S. Mondal, K. Bankura and D. Mishra, *Inorg. Chim. Acta*, 2019, **496**, 119069.
33 L. Hou, Y. Song, Y. Xiao, R. Wu and L. Wang, *Talanta*, 2020, **209**, 120534.
34 M. Saif, H. F. El-Shafiy, M. M. Mashaly, M. F. Eid, A. I. Nabeel and R. Fouad, *J. Mol. Struct.*, 2018, **1161**, 26–33.
35 Z. F. Pu, Q. L. Wen, Y. J. Yang, X. M. Cui, J. Ling, P. Liu and Q. E. Cao, *Spectrochim. Acta, Part A*, 2020, **229**, 117944.
36 D. M. Arvapalli, A. T. Sheardy, K. C. Alapati and J. Wei, *Talanta*, 2020, **209**, 120538.

